Proceedings of the 2003 IEEE International Frequency Control Symposium and PDA Exhibition
Jointly with the 17th European Frequency and Time Forum

INFLUENCE OF AUTOMATIC LEVEL CONTROL ON MICROMECHANICAL RESONATOR OSCILLATOR PHASE NOISE

Seungbae Lee and Clark T.-C. Nguyen
Center for Wireless Integrated Microsystems
Department of Electrical Engineering and Computer Science
University of Michigan, Ann Arbor, MI 48109-2122, U.S.A.

ABSTRACT

Clear differences in the phase noise performance of a 10 MHz MEMS-based micromechanical resonator oscillator have been measured using sustaining circuits with and without automatic-level control (ALC), and with differing mechanisms for ALC. In particular, low output power oscillators referenced to high-Q clamped-clamped beam μmechanical resonators exhibit an unexpected $1/f^3$ phase noise component without ALC, a $1/f^5$ phase noise component when an ALC circuit based on resonator dc-bias adjustment is used, and finally, removal of these components when an ALC circuit based on sustaining amplifier gain control is used, in which case the expected $1/f^2$ phase noise component is all that remains. That ALC is able to remove the $1/f^3$ phase noise seen in non-ALC'ed oscillators suggests that this noise component emanates primarily from nonlinearity in the voltage-to-force capacitive transducer, either through direct aliasing of amplifier $1/f$ noise, or through instabilities introduced by spring softening (i.e., Duffing) phenomena.

Keywords: MEMS, resonator, oscillator, phase noise, automatic level control, nonlinear

I. INTRODUCTION

Due to their great potential for direct integration or bonded merging with transistors onto single chips [1]-[4], electrostatically transduced vibrating micromechanical ("μmechanical") resonators have become increasingly attractive as frequency-setting elements in precision reference oscillators for communication applications. In particular, phase noise performance close to the requirements of the GSM cellular telephone standard has recently been demonstrated via an oscillator referenced to an extensional-mode single-crystal silicon vibrating bar with a Q of 200,000, constructed using an SOI process with a thick device layer [5]. Although the resonator used in [5] lacked adequate temperature stability, another resonator based on surface micromachined polysilicon structural material was recently demonstrated with a temperature coefficient as low as -0.24 ppm/^{o}C [6], a Q of 4,000 at 10 MHz, and a proven integrability with transistor electronics [1][4]. However, an oscillator based on this polysilicon resonator exhibited a $1/f^3$ phase noise component farther from the carrier than expected that prevented the oscillator from achieving GSM-like phase noise specifications [7].

Guided by a theoretical prediction that the observed $1/f^3$ phase noise component arises from resonator nonlinearity, this work attempts to remove $1/f^3$ phase noise by limiting the vibration amplitude of a polysilicon micromechanical resonator tank element (similar to the one used in [6]) in order to keep it in a linear operating region. In doing so, clear differences in the phase noise performance of a 10 MHz MEMS-based micromechanical resonator oscillator have been measured using sustaining circuits with and without automatic-level control (ALC), and with differing mechanisms for ALC. In particular, low output power oscillators referenced to high-Q clamped-clamped beam μmechanical resonators exhibit an unexpected $1/f^3$ phase noise component when ALC is not used, a $1/f^5$ phase noise component when an ALC circuit based on resonator dc-bias adjustment is used, and finally, removal of these components when an ALC circuit based on sustaining amplifier gain control is used, in which case the expected $1/f^2$ phase noise component is all that remains.

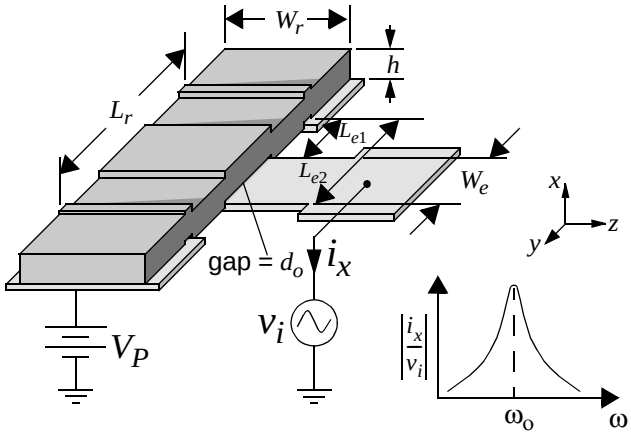

Fig. 1: Perspective-view schematic of a one-port clamped-clamped beam vibrating micromechanical resonator.

This paper details the design and implementation of the described automatic level controlled polysilicon micromechanical resonator oscillators utilizing series oscillator circuit topologies and off-chip active circuitry. Section II begins with modeling of the micromechanical resonator frequency-setting tank element, specifying its equivalent circuit model and deriving expressions that govern its power handling ability. Series oscillator topologies and ALC circuits are then presented in Section III and Section IV, along with theoretical models for the expected phase noise performance of these circuits. The paper then proceeds with experimental evaluations for each ALC oscillator design from Section V, culminating in a phase noise measurement proving that ALC can effectively remove $1/f^3$ phase noise components seen in non-ALC'ed oscillators.

II. MICROMECHANICAL RESONATOR MODELING

Figure 1 presents the perspective-view schematic of the one-port clamped-clamped beam ("CC-beam") vibrating micromechanical resonator used for this work, identifying key features and showing a bias and excitation configuration suitable for use in a series oscillator topology. As shown, this device is driven electrostatically via a combination of a dc-bias V_P applied through an inductor to the beam structure, and

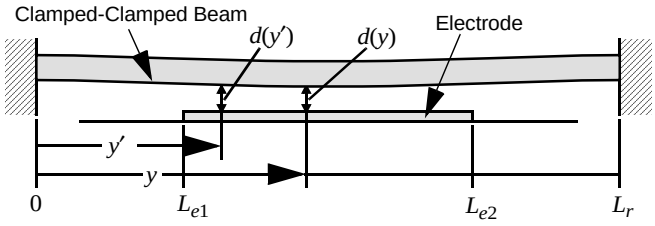

Fig. 2: Resonator cross-sectional schematic for frequency-pulling and impedance analysis.

an ac excitation v_i applied to its input electrode. For values of $V_P >> v_i$, this input voltage configuration results in an ac force at the frequency of v_i given (in phasor form) by

$$F_i = V_P \frac{\partial C}{\partial x} V_i \tag{1}$$

where V_i is the phasor input voltage (i.e., the voltage amplitude in this case), ε_o is the permittivity in vacuum, dimensional parameters are defined in Fig. 1, and $\partial C/\partial x$ is the integrated change in electrode-to-resonator overlap capacitance per unit displacement, given by (referring to Fig. 2)

$$\frac{\partial C}{\partial x} = \sqrt{\int_{L_{e1}}^{L_{e2}} \int_{L_{e1}}^{L_{e2}} \frac{(\varepsilon_o W_r)^2}{[d(y')d(y)]^2} \frac{k_{re}}{k_r(y')} \frac{X_{mode}(y)}{X_{mode}(y')} dy'dy} \tag{2}$$

where $k_r(y)$ is stiffness as a function of beam location y (to be defined later), k_{re} is the effective lumped stiffness at the beam location centered over the electrode, $d(y)$ is the gap spacing as a function y, which is not constant due to beam bending under the dc-bias electrostatic load, L_{e1} and L_{e2} are the y locations of the left and right edges of the electrode, and

$$X_{mode}(y) = \zeta(\cos ky - \cosh ky) + (\sin ky - \sinh ky) \tag{3}$$

describes the mode shape of a CC-beam. For the fundamental mode used in this work, k=4.730/L_r and ζ=–1.01781.

When the frequency of v_i matches the resonance frequency of the clamped-clamped beam, the beam is then driven into resonance with a resonance vibration amplitude given by

$$X = \frac{QF_i}{jk_{re}} = \frac{Q}{jk_{re}} \frac{\partial C}{\partial x} V_P V_i \tag{4}$$

where Q is the quality factor of resonator. Once in motion, a dc-biased (by V_P) time-varying capacitor is generated between the electrode and conductive resonator beam that sources a current through the device given by

$$I_o = V_P \frac{\partial C}{\partial x} \frac{\partial x}{\partial t} = \omega_o \frac{Q}{k_r} \left(\frac{\partial C}{\partial x}\right)^2 V_P^2 V_i \tag{5}$$

A. Resonance Frequency

To account for a wide range of length-to-width and length-to-thickness ratios, the beam dimensions for the clamped-clamped boundary condition of Fig. 1 that yield a specified resonance frequency are best found by solving the Timoshenko equations [8]

$$\tan\frac{\beta}{2} + \frac{\beta}{\alpha}\left(\frac{\alpha^2 + g^2(\kappa G/E)}{\beta^2 - g^2(\kappa G/E)}\right)\tanh\frac{\alpha}{2} = 0 \tag{6}$$

where E and ρ are the Young's modulus and density of the beam material, respectively, and

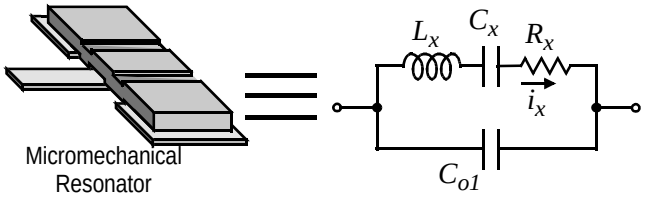

Fig. 3: One-port micromechanical resonator with its general electrical equivalent circuit

$$g^2 = \omega_{nom}^2 L_r^2 \left(\frac{\rho}{E}\right) \quad , I_r = \frac{W_r h^3}{12} \quad , G = \frac{E}{2(1+\nu)} \tag{7}$$

$$\left.\begin{matrix}\alpha^2 \\ \beta^2\end{matrix}\right\} = \frac{g^2}{2}\left[\mp\left(1 + \frac{E}{\kappa G}\right) + \sqrt{\left(1 - \frac{E}{\kappa G}\right)^2 + \frac{4L_r^2 h W_r}{g^2 I_r}}\right] \tag{8}$$

where ω_{nom} is the nominal radian resonance frequency (=2πf_{nom}) of the clamped-clamped beam with no dc-bias V_P applied, hence no frequency pulling due to electrical spring stiffness [10]; I_r is the bending moment of inertia; G and ν are the shear modulus of elasticity and Poisson's ratio, respectively, of the structural material; κ is the shear-deflection coefficient; and all other variables and axis definitions are indicated in Fig. 1.

Again, the variable f_{nom} represents the mechanical resonance frequency for the case of zero DC bias (i.e., V_P=0) applied to the resonator body. As described in the past literature [10][9], the resonance frequency of a capacitively-transduced beam is a function of the DC-bias voltage V_P applied to the resonator body, which effectively introduces an electrical spring stiffness that subtracts from the mechanical stiffness of the beam. The resonance frequency f_o of a clamped-clamped beam device including the effect of DC-bias-derived electrical stiffness is given by

$$f_o = f_{nom}\left[1 - \left\langle\frac{k_e}{k_m}\right\rangle\right]^{1/2} \tag{9}$$

where $\langle k_e/k_m \rangle$ is a parameter representing the effective electrical-to-mechanical stiffness ratio integrated over the electrodes, given by

$$\left\langle\frac{k_e}{k_m}\right\rangle = \int_{L_{i1}}^{L_{i2}} \frac{V_P^2 \varepsilon_o W_r}{[d(y)]^3 k_m(y)} (dy) \tag{10}$$

where $k_m(y)$ is the purely mechanical stiffness as a function of location y on the μresonator beam [9], given by

$$k_m(y) = [2\pi f_{nom}]^2 m_r(y) \tag{11}$$

where $m_r(y)$ is the equivalent mass at a location y, to be given later. Note that $k_m(y)$ differs from $k_r(y)$ in that the latter (to be defined shortly) includes the effect of dc-bias V_P.

B. Electrical Equivalent Circuit

To facilitate transistor-level oscillator design, the electrical performance of a one-port vibrating micromechanical resonator can be modeled by an equivalent *LCR* circuit, as shown in Fig. 3. Equations for the element values in this circuit have already been developed in [9] and are summarized here (with reference to Fig. 2) for reader convenience:

Table I: Micromechanical Resonator Design Summary

Parameter	V_P = 5.5V	V_P = 12V	Units
Young's Modulus of PolySi, E	150	150	GPa
Density of Polysilicon, ρ	2,300	2,300	kg/m^3
Structural Layer Thickness, h	2.04	2.04	μm
μRes. Beam Length, L_r	40	40	μm
μRes. Beam Width, W_r	10	10	μm
Electrode Width, W_{e2}	26	26	μm
Electrode-to-μRes. Gap, d_o	1,315	1,315	Å
Resonator Mass @ I/O, m_{re}	7.44×10^{-13}	7.44×10^{-13}	kg
Resonator Stiffness @ I/O, k_{re}	3300	3300	N/m
Calc. Equiv. Inductance, L_x	2.37	0.5	H
Calc. Equiv. Resistance, R_x	58	12	kΩ
Calc. Equiv. Capacitance, C_x	0.01	0.46	fF
Static Overlap Capacitance, C_o	18.8	18.8	fF
Meas. Quality Factor, Q	2,700	2,700	—
Meas. Center Frequency, f_o	10.56	10.72	MHz
Meas. Series Resistance, R_x	53	11	kΩ

$$R_x = \frac{\sqrt{k_{re}m_{re}}}{Q\eta_e^2}\ ,\ L_x = \frac{m_{re}}{\eta_e^2}\ ,\ C_x = \frac{\eta_e^2}{k_{re}} \tag{12}$$

where k_{re} and m_{re} are the equivalent stiffness and mass at the centers of the electrodes obtained by evaluating [9]

$$m_r(y) = \frac{\rho W_r h\int_0^{L_r}[X_{mode}(y')]^2(dy')}{[X_{mode}(y)]^2}\ ,\ k_r(y) = \omega_o^2 m_r(y) \tag{13}$$

at y's corresponding the centers of the electrodes; and η_e is the electromechanical coupling factor, given by

$$\eta_e = V_P\frac{\partial C}{\partial x}. \tag{14}$$

Table I summarizes the *LCR* equivalent circuit elements for the specific clamped-clamped beam micromechanical resonator design used in this work at the two dc-bias levels used. Compared with the R_x=15 Ω, L_x=10 mH, and C_x=26 fF typically exhibited by quartz crystals, the element values for this 10 MHz resonator are quite large and will impose different requirements on the circuits used to sustain their oscillation.

III. Oscillator Design

For ease in construction (due to the availability of a readily usable off-chip sustaining amplifier), and for good noise performance and stability, a series resonant oscillator configuration [1][11] is used in this work. Figure 4 presents the basic series type ALC oscillator topology utilized to instigate, sustain, and limit oscillation. Here, the micromechanical resonator is embedded in a positive feedback loop with a transresistance amplifier that possesses sufficient gain to initiate and sustain oscillation. Since the micromechanical resonator used for this work is a one-port device (as opposed to the two port devices used in a previous lower frequency design [1]), a bias tee is now required to allow the resonator structure to both accept a dc-bias voltage V_P and simultaneously serve as the output electrode delivering current to the input port of the sustaining transimpedance amplifier.

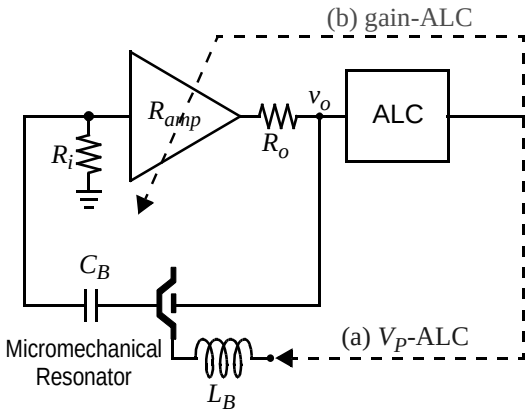

Fig. 4: General schematic for the series oscillators with two ALC circuit options: (a) one that adjusts the micromechanical resonator dc-bias V_P (V_P-ALC); or (b) one that adjusts the sustaining amplifier gain (gain-ALC).

Ignoring the ALC loops for now, the two basic requirements for start-up of oscillation in this series oscillator configuration are:

(1) The sustaining amplifier transimpedance gain R_{amp} must be larger than the total series resistance in the loop, or

$$R_{amp} > R_x + R_i + R_o \tag{15}$$

(2) The total phase shift around the positive feedback loop must be 0^o (or 360^o).

For best stability, the second of the above criteria is best satisfied when the phase shift through the micromechanical resonator is as close to 0^o as possible, since this is where its phase versus frequency curve has its greatest slope, and is thus the point where the resonator can best suppress frequency instabilities caused by phase shifts (due to noise, temperature shifts, etc. ...) across the sustaining amplifier. The above in turn implies that best stability is achieved when the phase shift across the sustaining amplifier at the oscillation frequency is also as close to 0^o as possible.

A. Oscillator Phase Noise

The phase noise density $L\{f_m\}$ at a given offset frequency f_m from the carrier f_o of an oscillator can be computed approximately using Leeson's equation [12]

$$L\{f_m\} = \frac{2kTF}{P_o}\cdot\left[1+\left(\frac{f_o}{2Q\cdot f_m}\right)^2\right] \tag{16}$$

where f_m is the offset from the carrier frequency at which phase noise is being evaluated, k is Boltzmann's constant, F is the noise figure of the sustaining amplifier, and P_o is the oscillator output power.

From the first term in (16), the output (or "carrier") power of a given oscillator clearly plays an important role in determining the phase noise performance, especially at large offset frequencies from the carrier, where the noise is not shaped by the Q of the resonator tank element. Thus, the far-from-carrier phase noise performance of an oscillator is a strong function

of its carrier power, which in turn, is limited by the amount of power its frequency-setting tank element can handle. Normally, this is not an issue for oscillators referenced to quartz crystals and other macroscopic tank elements, for which the output carrier power is often limited not by the tank element, but by the sustaining amplifier circuit. However, due to their tiny size, present micromechanical resonators have a smaller power threshold than their macroscopic counterparts, to the point where now it is the resonator, not the sustaining circuit, that dictates the maximum oscillator carrier power.

A quantitative understanding of which design parameters are most responsible for setting the power handling limits of a clamped-clamped beam micromechanical resonator can be obtained by finding an expression for the power through the device when it vibrates at its maximum amplitude, assumed to be some fraction of the electrode-to-resonator gap spacing

$$X_{max} = a d_o , \tag{17}$$

where a should < 0.56 for a capacitively driven μmechanical resonator without charge feedback to extend its range.

Inserting (17) into (5), and using the approximation

$$\frac{\partial C}{\partial x} = \frac{\varepsilon_o W_r W_e}{d_o^2} \tag{18}$$

which ignores stiffness and gap spacing variations along the beam length, the expression for the current through a capacitively-transduced clamped-clamped beam micromechanical resonator at maximum vibration amplitude is

$$I_{omax} = \omega_o V_P \frac{\varepsilon_o W_r W_e}{d_o} a . \tag{19}$$

Using (19), an expression for the corresponding maximum power through the resonator can be written as

$$P_{omax} = I_{omax}^2 R_x = \omega_o a^2 \frac{k_r}{Q} d_o^2 . \tag{20}$$

From (20), a larger power handling capability for a capacitively-transduced clamped-clamped beam micromechanical resonator can be attained by increasing in its frequency, stiffness, and electrode-to-resonator gap spacing, or decreasing its Q. The latter requirement obviously contradicts the requirement for high Q for good close-to-carrier phase noise, and indicates that Q can be traded-off between close-to-carrier and far-from-carrier phase noise needs.

B. 1/f³ Phase Noise

Without automatic level control (ALC), the amplitude of an oscillator limits by the action of nonlinearity in either its sustaining amplifier circuit or its resonator tank. As previously mentioned, micromechanical resonator oscillators differ from the vast majority of macroscopic resonator oscillators in that the resonator, not the sustaining amplifier, provides the nonlinearity that limits the oscillation amplitude in a non-ALC'ed oscillator. Unfortunately, as described in [7], limiting via resonator nonlinearity generates an unexpected $1/f^3$ phase noise component that has so far prevented micromechanical resonator oscillators from meeting the phase noise requirements of today's cellular communication standards.

A quantitative understanding of the origins of $1/f^3$ phase noise in a non-ALC'ed micromechanical resonator oscillator can be obtained by considering one possible mechanism, where $1/f$ noise in the sustaining electronics is aliased into the oscillator output band by nonlinearity in the resonator's capacitive transducer. An analytical derivation that assumes this mechanism yields the following expression for phase noise [7]

$$L\{f_m\} = \frac{1}{4Q_l^2}\frac{1}{V_P^2}\left[\frac{1}{4} + \frac{Q_l^2}{k_{reff}^2}\frac{(\varepsilon_o A_o)^2}{d_o^6} V_P^4\right] \cdot 2qK_1 I_B R_s^2 \cdot \frac{f_o^2}{f_m^3} \tag{21}$$

where Q_l is the loaded quality factor of the resonator, K_1 is the $1/f$ noise constant of the bipolar transistor assumed to be at the input of the sustaining transimpedance amplifier (which is the case for the NE5211), I_B is the base current of this input bipolar transistor, and $R_s = R_x + R_i + R_o$. This expression will be used later in search of the origins of $1/f^3$ phase noise.

IV. Automatic Level Control

To investigate and remove the described $1/f^3$ phase noise phenomenon, this work uses automatic level control to avoid limiting via resonator nonlinearity and insure that the resonator operates in a linear region. The basic method for ALC used here entails measuring the amplitude of oscillation, comparing it with a reference amplitude, then feeding back a control signal (proportional to the difference between the amplitude and reference) to elements of the oscillator circuit that can regulate its oscillation amplitude. Two different regulating mechanisms are explored here:

(1) The series motional resistance R_x of the resonator is controlled by adjusting the dc-bias V_P applied to the micromechanical resonator—a method to be referred to as "V_P-ALC" in this paper; and

(2) the gain of the sustaining amplifier is controlled by adjusting the value of a gain-setting element or variable in the sustaining amplifier—a method to be referred to as "gain-ALC" in this paper.

Specific implementations for each of the above methods are now detailed.

A. V_P-ALC Oscillator

Figure 5 presents the implementation schematic for the V_P-ALC'ed μmechanical resonator series oscillator circuit. Here, an NE5211 single-ended input to differential output transimpedance amplifier provides a transresistance gain of 14 kΩ to instigate and sustain oscillation. The oscillation voltage amplitude (or μresonator vibration amplitude) is controlled by automatically adjusting the dc-bias V_P applied to the resonator, and changing its series motional resistance R_x until the oscillation voltage amplitude matches or is proportional to a preset voltage V_{limit}.

Because the output voltage of the base oscillator circuit (taken from one output of the NE5211) is on the order of only 3 mV with ALC engaged, a low noise amplifier (LNA) is used to boost the output signal to v_{oLNA} before sending it to measurement instrumentation and to the ALC loop. Once directed to the ALC loop, the oscillation output voltage v_{oLNA} is half-wave rectified through a super-diode configuration, then low pass filtered by a simple RC circuit, after which, a signal with a dc level V_{oLNA} equal to the peak amplitude of v_{oLNA} results. This dc level is then compared with a preset voltage V_{limit}, and the difference between them weighted and subtracted (in magnitude) from the dc voltage V_{PB} in the bias voltage control circuit to generate the V_P applied to the μmechanical resonator. Note that the bias voltage controller in Fig. 5 also filters out

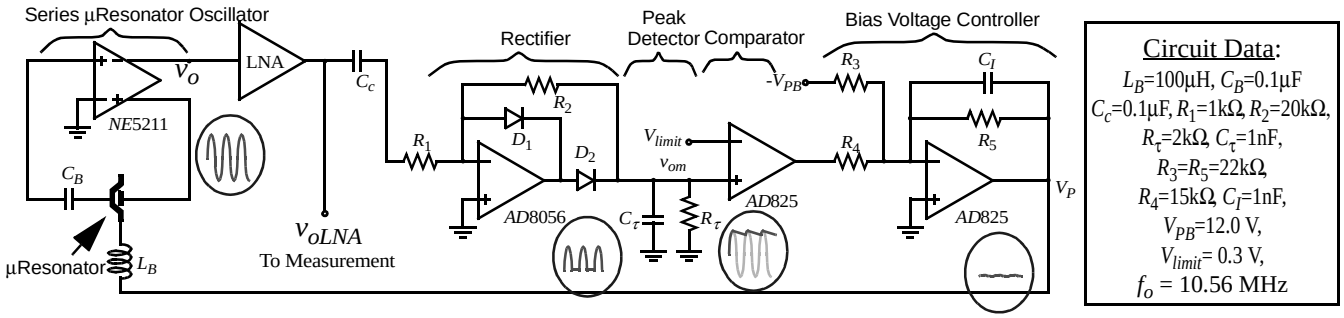

Fig. 5: Implementation circuit schematic for a micromechanical resonator oscillator using an automatic level control circuit that limits the oscillation amplitude by controlling the dc-bias voltage V_P applied to the resonator—referred to as "V_P-ALC" in this paper.

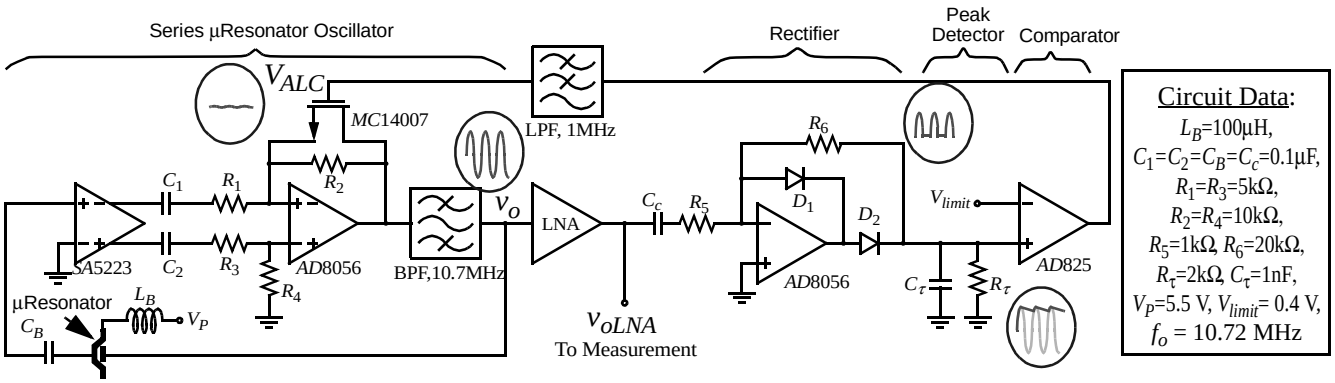

Fig. 6: Implementation circuit schematic for a micromechanical resonator oscillator using an automatic level control circuit that limits the oscillation amplitude by controlling the gain of the sustaining amplifier—referred to as "gain-ALC" in this paper.

any high frequency noise present in V_P, preventing this noise from reaching the μmechanical resonator, where it could compromise the frequency stability of the oscillator via electrical stiffness-based frequency pulling [9][10].

The V_P-ALC circuit of Fig. 5 acts by lowering the V_P of the micromechanical resonator as the oscillation amplitude builds, increasing its series motional resistance R_x in such a way that

$$R_x = R_{amp} - R_i - R_o , \tag{22}$$

when V_{oLNA} matches V_{limit}. When (22) is met, the loop gain of the circuit is unity, and the oscillation amplitude ceases to grow, staying locked (by feedback action) at a value given by

$$V_o = \frac{V_{limit}}{A_{vLNA}} \tag{23}$$

where A_{vLNA} is the voltage gain of the LNA.

B. Gain-ALC Oscillator

Figure 6 presents the implementation schematic for the gain-ALC'ed μmechanical resonator series oscillator circuit. Here, an off-chip implementation using available electronics was again desired, but the NE5211 transimpedance amplifier could no longer be used, since its gain is not easily accessible. Thus, a two-stage amplifier circuit is used instead that combines an SA5223 transresistance amplifier with a differential gain of 125 kΩ, together with a gain-controllable differential second stage amplifier using an AD8056 operational amplifier and resistive feedback to supply an additional gain of 2 or less, for a total gain of 250 kΩ. The gain control mechanism used in the second stage is similar to that in [1], where the shunt-shunt feedback element consists of a large start-up resistor R_2 in parallel with an MOS resistor MC14007, for which the channel resistance is controllable by adjustment of its gate voltage. Due to the use of high gain off-chip components to make this board-level oscillator, a 10.7 MHz bandpass filter with a 3.8 MHz bandwidth is also included in the oscillator loop to suppress spurious gain paths that could generate oscillations around stray inductance and capacitance.

Although its implementation is slightly different, the basic mechanism for ALC in the design of Fig. 6 is similar to that for the V_P-ALC'ed oscillator of Fig. 5 in that the oscillation amplitude is first sensed via a super-diode-based envelope detector circuit, then compared with a reference voltage V_{limit} to generate the dc signal that feeds back to the gate of MC14007 to control its channel resistance, hence, control the gain of the second stage. The overall circuit is designed so that when the oscillator is first powered on, the ALC circuit delivers a voltage to the gate of MC14007 that is smaller than its threshold voltage, giving it a channel resistance much larger than R_2. In their parallel configuration, R_2 thus determines the gain of the sustaining circuit during start-up of the oscillator. As the oscillation amplitude grows, the ALC circuit increases MC14007's gate voltage, which lowers its channel resistance, hence lowers the shunt-shunt impedance of the second stage, and thereby reduces the gain of sustaining amplifier. When V_{oLNA} matches V_{limit}, the action of the feedback sets the total transimpedance gain of the loop to

$$R_{amp} = R_x + R_i + R_o \quad , \tag{24}$$

at which point the loop gain of the circuit is unity, and the oscillation amplitude stays locked (by feedback) at a value given again by (23).

It should be noted that the gain of the gain-ALC'ed oscillator of Fig. 6 is purposely made quite large in order to accommodate resonators with higher stiffnesses k_r and larger

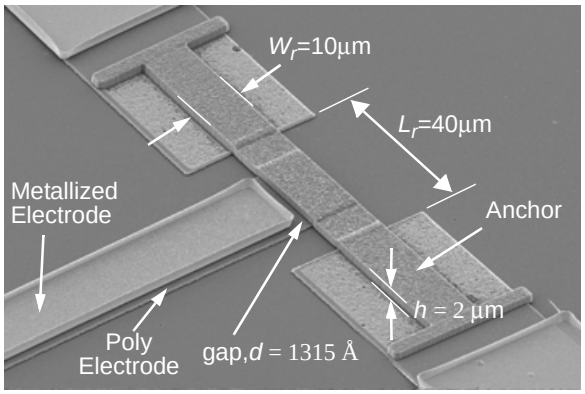

Fig. 7: SEM of a surface-micromachined 10-MHz vertical clamped-clamped beam polysilicon μmechanical resonator.

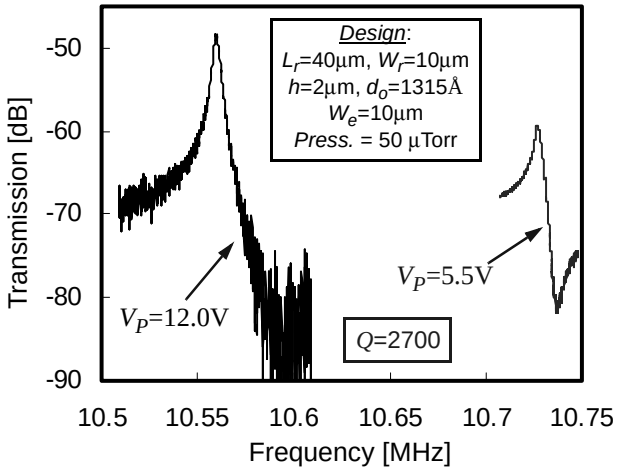

Fig. 8: Measured frequency response spectra for a ~10 MHz polysilicon vertical clamped-clamped beam μmechanical resonator at two different dc-biases.

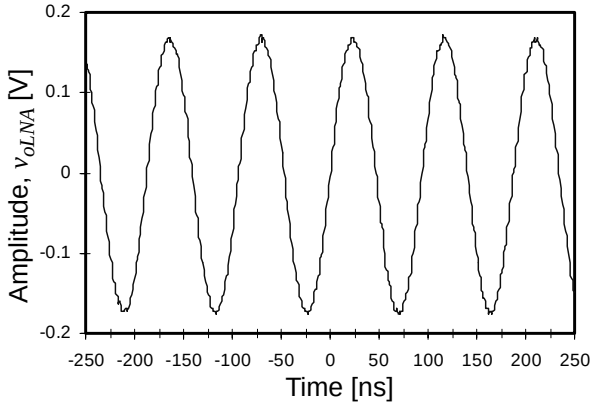

Fig. 9: V_P-ALC μresonator oscillator output waveform (taken at the output of the LNA, which had a A_{vLNA}=50).

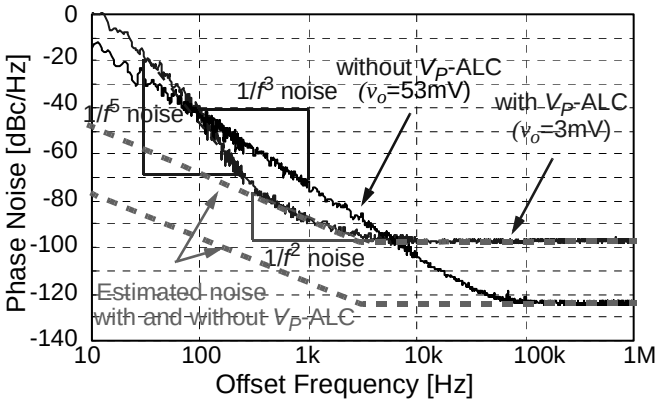

Fig. 10: Measured phase noise power spectral density-to-carrier power ratio versus frequency offset from the carrier for the V_P-ALC μmechanical resonator oscillator of Fig. 5 with and without ALC engaged. The estimated noise curves were generated using (16) with the measured oscillation amplitudes.

electrode-to-resonator gap spacings d_o, hence higher motional resistances R_x's, which, as shown in Section III, should be capable of achieving better far-from-carrier phase noise due to higher power handling.

V. Experimental Results

10-MHz clamped-clamped beam micromechanical resonators designed as summarized in Table I were fabricated using a small-gapped vertical resonator process similar to that described in [9]. Figure 7 presents the scanning electron micrograph (SEM) of one such resonator, identifying key features and dimensions. Figure 8 presents frequency spectra measured for this resonator under 50 μTorr pressure in a custom-built vacuum chamber and under different values of dc-bias, where the dependence of the resonance frequency and output signal level on dc-bias V_P are clearly seen, and are consistent with the predictions of Section II. From the measured curves, series motional resistances of 11 kΩ and 53 kΩ are exhibited with V_P=12 V and V_P=5.5 V, respectively. Table I summarizes the element values for the complete equivalent circuits and other measured parameters for this resonator under these two bias levels.

The oscillator circuits of Figs. 5 and 6 were implemented on printed circuit (pc) boards shaped to allow placement within the custom-built vacuum chamber. Dies containing fabricated clamped-clamped beam μmechanical resonators were glued to these boards over specially grounded regions. Connections between individual devices on each die to appropriate board-level circuits were made via bond wires from die bond pads to board bond pads, all in an effort to minimize interface parasitics. Connections between pc board electronics within the vacuum chamber and external biasing and measurement instrumentation were established via special, sealed electrical feedthroughs designed into the custom vacuum chamber.

A. V_P-ALC Oscillator Performance

Because the V_P-ALC'ed oscillator possesses only a small amount of transimpedance gain (only 14 kΩ), the series motional resistance R_x of the micromechanical resonator used as its tank element must be smaller than 14 kΩ to allow start-up of oscillation. To attain a sufficiently small R_x, a dc-bias voltage of 12V was needed, at which voltage the resonator takes on the characteristics summarized in the second column of Table I. Figure 9 presents the output signal waveform measured on an oscilloscope for the circuit of Fig. 5 with the resonator V_P set at 12V. Here, the measured oscillator output frequency matches the 10.56 MHz measured in Fig. 8 for the V_P=12V case, verifying that the micromechanical resonator does indeed set the frequency of the oscillator.

Figure 10 presents plots of phase noise density versus frequency offset from the 10.56 MHz carrier, measured using an HP E5500 Phase Noise Measurement system, for the oscilla-

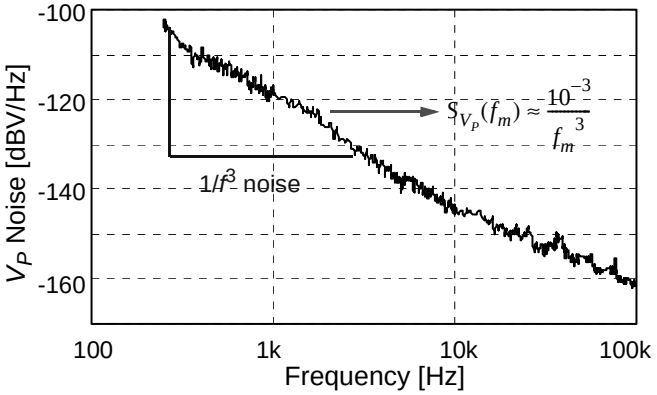

Fig. 11: V_P noise spectral density at the output of the ALC circuit in the V_P-ALC µmechanical resonator oscillator.

tor of Fig. 5 with and without the V_P-ALC circuit hooked up. As shown, when the circuit is operated without ALC, the oscillation voltage amplitude limits via resonator nonlinearity to a value of 53 mV. When allowed to reach this value of amplitude, the far-from-carrier phase noise floor reaches down to −123 dBc/Hz. However, as advertised in Section I, a $1/f^3$ phase noise component is seen at offsets closer to the carrier that dominates among noise mechanisms, degrading the phase noise to a value as poor as −74 dBc/Hz at a 1 kHz offset from the carrier.

Once the dc-bias-adjusting ALC is interconnected, the amplitude of the vibrating micromechanical resonator limits such that the oscillation voltage amplitude now limits to only 3 mV, and the $1/f^3$ phase noise component disappears—a behavior that seems to support a resonator-nonlinearity-based mechanism for the generation of $1/f^3$ phase noise. With the $1/f^3$ phase noise removed, the expected $1/f^2$ phase noise component can now be seen at carrier offsets from about 400 Hz to 5 kHz. Using the data from Table I, (16) predicts a phase noise of −91 dBc/Hz at 1 kHz offset, which is very close to the −97 dBc/Hz measured in Fig. 10, giving added confidence in (16). In addition, the corner frequency where the $1/f^2$ phase and noise floor meet is calculated to be $f_o/(2Q)$= 2.5 kHz, which is also close to the ~2.4 kHz measured in Fig. 10.

Unfortunately, in the process of removing $1/f^3$ noise, the V_P-ALC circuit seems to have introduced a new phase noise component for offsets below 400 Hz, which seems to follow a $1/f^5$ dependence. The origins of this $1/f^5$ phase noise are consistent with a mechanism where $1/f$ noise at the ALC circuit output superimposes itself on the dc-bias voltage V_P applied to the resonator and generates frequency jitter by causing instantaneous shifts in the V_P-generated electrical stiffness [9] that contributes to determining the overall resonance frequency of the micromechanical device.

To quantitatively verify this electrical stiffness-based mechanism, the expression for phase noise generated by V_P noise can be derived using (9) to be

$$L\{f_m\}\big|_{V_P} = \frac{1}{4V_P^{\,2}} \cdot \frac{\langle \frac{k_e}{k_m} \rangle^2}{1 - \langle \frac{k_e}{k_m} \rangle} \cdot \left(\frac{f_o}{f_m}\right)^2 \cdot S_{V_P}(f_m) \qquad (25)$$

where $S_{V_P}(f_m)$ is the noise spectral density at the output of the V_P-generating ALC circuit. As shown in Fig. 11, which plots

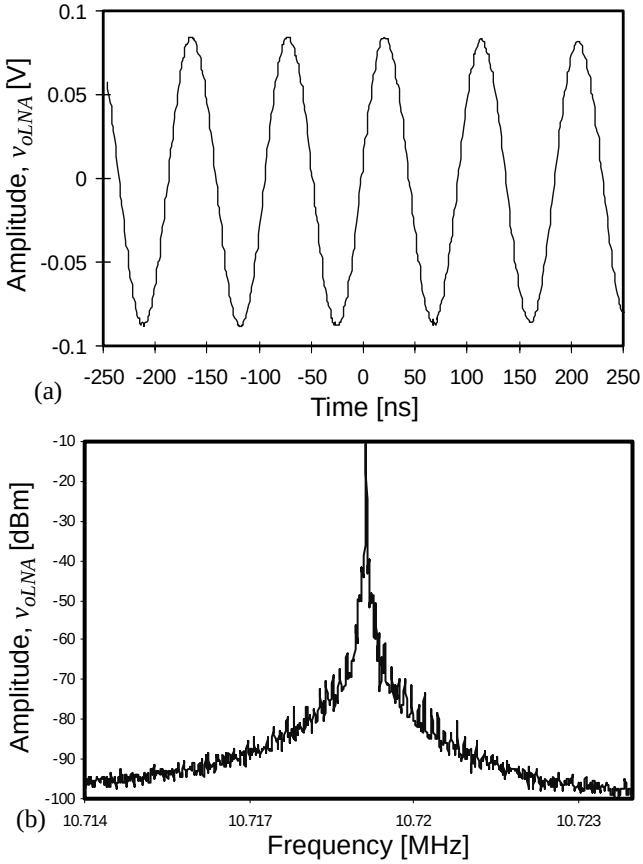

Fig. 12: Measured output (a) waveform and (b) spectrum (taken at the output of the LNA, which had a gain A_{vLNA}=1) for the gain-ALC µmechanical resonator oscillator of Fig. 6.

the measured ALC output noise spectral density $S_{V_P}(f_m)$, the noise on the V_P signal applied to the resonator goes as $1/f^3$, which when inserted into (25) yields an overall $1/f^5$ phase noise component consistent with the data of Fig. 10. This strongly supports the above electrical stiffness-based mechanism for generation of $1/f^5$ phase noise.

B. Gain-ALC Oscillator Performance

As mentioned in Section IV, the gain-ALC oscillator design has several advantages over the V_P-ALC, including a substantially higher gain and no direct connection to the frequency-setting micromechanical resonator. As such, the gain-ALC circuit is expected to be able to achieve better far-from-carrier phase noise (provided a higher power handling resonator with a larger k_{re} and d_o is used), and is expected not to generate $1/f^5$ phase noise.

For the gain-ALC oscillator design, oscillations start to build up when the micromechanical resonator dc-bias reaches V_P=5.5V, which is much lower than the voltage required for the previous V_P-ALC circuit, and which corresponds to a resonator R_x=53 kΩ. Figures 12(a) and (b) present the oscilloscope waveform and output spectrum, respectively, of this oscillator in steady-state, both measured at the output of the LNA in Fig. 5. These data show an oscillation frequency that matches the 10.72 MHz of the V_P=5.5V curve in Fig. 8, and a much larger oscillation amplitude of 90 mV that should yield a much improved far-from-carrier phase noise performance.

Figure 13 presents the phase noise density spectrum of this

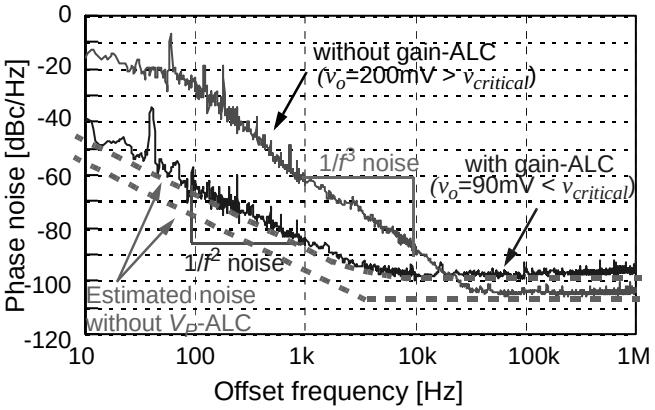

Fig. 13: Measured phase noise power spectral density-to-carrier power ratio versus frequency offset from the carrier for the gain-ALC μmechanical resonator oscillator of Fig. 6 with and without ALC engaged. The estimated noise curves were generated using (16) with the measured oscillation amplitudes.

oscillator as measured at the LNA output using an HP E5500 Phase Noise Measurement system, with and without the gain-ALC circuit. With a higher amplitude of oscillation, the far-from-carrier phase noise density of the gain-ALC'ed oscillator is now −97 dBc/Hz, which is closer to non-ALC'ed value of −105 dBc/Hz. This performance is several tens of dB short of requirements for cellular communications, and is caused by the extremely bad noise performance of the electronic components making up the sustaining oscillator. (This should be obvious, as the far-from-carrier noise performance of the non-ALC'ed version of this oscillator is many times worse that of the non-ALC'ed version of the V_P-ALC circuit.) Improvements in the sustaining amplifier design, combined with the methods for improving far-from-carrier phase noise through resonator design described in Section III, should be able to greatly improve the spectrum of Fig. 13.

Perhaps more important at the present time is that the gain-ALC oscillator circuit completely removes the $1/f^3$ phase noise component that plagues the non-ALC'ed version of this oscillator, reducing the phase noise density at 1 kHz offset from the 10.72 MHz carrier down to −85 dBc/Hz. This is also far short of the required −120 dBc/Hz at 1 kHz offset, but again, methods for improving this are available through (20), as discussed in Section III. In particular, the use of a resonator with a higher Q, such as a substrate-isolated free-free beam [14], and with a larger thickness and transducer gap spacing, should greatly improve the performance seen in Fig. 13.

It should be noted in passing that scaling-induced noise limitations, such as adsorption-desorption or temperature fluctuation noise, are not problematic for the micro-scale (as opposed to nano-scale) resonators of this work [7].

VI. Origins of $1/F^3$ Phase Noise

The circuits of the previous section not only help to remove the $1/f^3$ phase noise that plagued previous non-ALC'ed micromechanical resonator oscillators, they also give clues to the mechanism behind its generation. In particular, the following observations can now be made for the case of oscillators referenced to capacitively-transduced micromechanical resonators:

(1) Since it can be removed by restricting oscillation amplitudes via ALC, $1/f^3$ phase noise occurs only for large micromechanical resonator vibration amplitudes.

(2) The fact that the non-ALC'ed oscillator of Fig. 6 still exhibits $1/f^3$ phase noise even with a 10.7 MHz band-pass filter (BPF) in its positive feedback loop suggests that $1/f^3$ phase noise is *not* derived from $1/f$ phase noise in the sustaining electronics, which should be removed by the BPF.

(3) Furthermore, for the case of the non-ALC'ed oscillator of Fig. 10, Eq. (21), which assumes an aliased $1/f$ noise mechanism for $1/f^3$ noise generation, yields a phase noise density at 1 kHz offset from the carrier of −103 dBc/Hz. This undershoots the actual measured noise of −74 dBc/Hz by several orders of magnitude.

Although the above observations are helpful in that they disqualify an aliased $1/f$ noise mechanism from being responsible for the measured $1/f^3$ phase noise, they still do not establish a mechanism for this noise component.

A. Duffing As a Mechanism For $1/f^3$ Phase Noise?

Interestingly, recent observations seem to tie $1/f^3$ phase noise to a spring-softening Duffing nonlinearity generated by a third-order effective electrical stiffness [13] between the electrode and resonator beam that dominates over any third-order mechanical stiffness. Quantitatively, when this phenomenon is considered, the force applied to the micromechanical resonator becomes a function of not only its mechanical stiffness k_m, but also of an electrical stiffness k_e, and can be expressed by [15]

$$f = (k_{m1} - k_{e1})x + (k_{m3} - k_{e3})x^3 \qquad (26)$$

where k_{m1} and k_{e1} model the linear mechanical and electrical spring constants, and k_{m3} and k_{e3} model their third-order spring nonlinearities. Through electrostatic analyses, approximate expressions for k_{e1} and k_{e3} can be derived as [15]

$$k_{e1} \approx V_P^2 \frac{\varepsilon_o W_r W_e}{d_o^3} \quad , \quad k_{e3} \approx V_P^2 \frac{\varepsilon_o W_r W_e}{d_o^5} \qquad (27)$$

Spring softening is observed when $k_{e3} > k_{m3}$ (i.e., when the third-order coefficient in (26) is negative), which is the case here, since the electrode-to-resonator gaps d_o are quite small for the resonators of this work.

Interestingly, the $1/f^3$ phase noise component seems to be observed only when the μresonator amplitude exceeds the critical point in its spring softening Duffing curve [13]. Figure 14 and 15 present frequency responses measured with increasing drive voltages for a CC-beam micromechanical resonator with V_P=12V and 5.5V, respectively. With V_P=12V in Fig. 14, Duffing appears for drive voltage amplitudes V_i over the critical value ($V_{critical}$ =19 mV). For a smaller V_P (=5.5V), the critical drive voltage ($V_{critical}$=122mV) increases, since k_{e3} (as defined by (27)) is smaller.

At present, a concrete link between spring-softened Duffing behavior and $1/f^3$ phase noise has not been established. However, mechanisms based on a link between these phenomena are plausible, for example, where the resonance frequency of a micromechanical resonator shifts between multiple permissible values near the critical point, generating oscillation frequency instability that might go as $1/f^3$. It is also not unreasonable to postulate that Duffing nonlinearity may also even be responsible for limiting the oscillation amplitude of

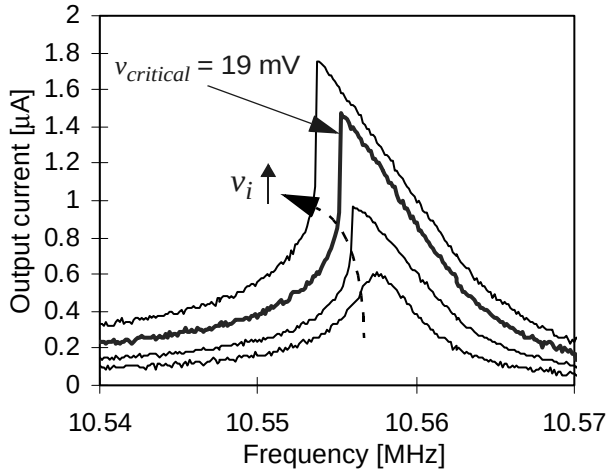

Fig. 14: Measured output current versus frequency plots for the micromechanical resonator of Fig. 7 with V_P=12V, showing spring-softening Duffing behavior as the vibration amplitude increases.

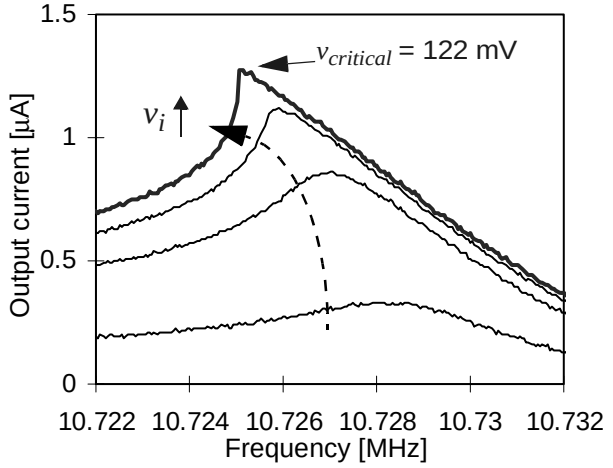

Fig. 15: Measured output current versus frequency plots for the micromechanical resonator of Fig. 7 with V_P=5.5V, showing spring-softening Duffing behavior as the vibration amplitude increases.

non-ALC'ed micromechanical resonator oscillators [15]. These hypotheses, however, are as yet unproven, and work continues to establish the actual mechanisms behind the generation of $1/f^3$ phase noise in non-ALC'ed micromechanical resonator oscillators.

VII. Conclusions

Clear differences in the phase noise performance of a 10 MHz MEMS-based micromechanical resonator oscillator have been measured using sustaining circuits with and without automatic-level control, and with two different mechanisms for ALC: one that controls the overall loop gain by adjusting the dc-bias applied to the resonator structure; and another that does so by adjusting the gain of the sustaining amplifier. Low output power oscillators referenced to high-Q clamped-clamped beam μmechanical resonators exhibit an unexpected $1/f^3$ phase noise component without ALC, a $1/f^5$ phase noise component when an ALC circuit based on resonator dc-bias adjustment is used, and finally, removal of these components when an ALC circuit based on sustaining amplifier gain control is used, in which case the expected $1/f^2$ phase noise component is all that remains close to the carrier.

Although mechanisms based on resonator transducer nonlinearity have been proposed, a mechanism behind the generation of $1/f^3$ phase noise in non-ALC'ed micromechanical resonator oscillators is still not established. Interestingly, the $1/f^3$ phase noise component seems to be observed only when the resonator amplitude exceeds the critical point in its spring softening Duffing curve, suggesting a Duffing nonlinearity-related noise generation mechanism. Work to isolate the cause of $1/f^3$ phase noise in non-ALC'ed oscillators continues. Whichever the mechanism, the removal by this work of the $1/f^3$ phase noise that plagued previous oscillators now makes the use of on-chip vibrating μmechanical resonator technology for frequency references much more plausible

***Acknowledgment*:** This work was supported under DARPA Cooperative Agmt. No. F30602-01-1-0573.

References:

[1] C. T.-C. Nguyen and R. T. Howe, "An integrated CMOS micromechanical resonator high-Q oscillator," *IEEE J. Solid-State Circuits*, vol. 34, no. 4, pp. 440-455, April 1999.

[2] T. A. Core, W. K. Tsang, S. J. Sherman, "Fabrication technology for an integrated surface-micromachined sensor," *Solid State Technology*, pp. 39-47, Oct. 1993.

[3] A. E. Franke, D. Bilic, D. T. Chang, P. T. Jones, T.-J. King, R. T. Howe, and G. C. Johnson, "Post-CMOS integration of germanium microstructures," *Tech. Digest*, 12th Int. IEEE MEMS Conf., Orlando, Florida, Jan. 17-21, 1999, pp. 630-637.

[4] A.-C. Wong, Y. Xie, and C. T.-C. Nguyen, "A bonded-microplatform technology for modular merging of RF MEMS and transistor circuits," *Dig. of Tech. Papers*, Transducers'01, Munich, Germany, June 10-14, 2001, pp. 992-995.

[5] T. Mattila, J. Kiihamaki, T. Lamminmaki, O. Jaakkoka, P. Rantakari, A. Oja, H. Seppa, H. Kattelus and I. Tittonen, "A 12 MHz micromechanical bulk acoustic mode oscillator," *Sensors and Actuators, A* 101, pp. 1-9, 2002

[6] W. -T. Hsu and C. T. -C. Nguyen, "Stiffness-compensated temperature-insensitive micromechanical resonators," *Tech. Digest*, 2002 IEEE Int. Micro Electro Mechanical Systems Conf., Las Vegas, Nevada, Jan. 20-24, 2002, pp. 731-734.

[7] S. Lee, M. U. Demirci, and Clark T.-C. Nguyen, "A 10-MHz micromechanical resonator Pierce reference oscillator for communications," *Digest of Technical Papers*, the 11th Int. Conf. on Solid-State Sensors & Actuators (Transducers'01), Munich, Germany, June 10-14, 2001, pp. 1094-1097.

[8] S. Timoshenko, D. H. Young, and W. Weaver Jr., *Vibration Problems in Engineering*, 5th ed. New York: Wiley, 1990.

[9] F. D. Bannon III, J. R. Clark, and C. T.-C. Nguyen, "High frequency micromechanical filters," *IEEE J. Solid-State Circuits*, vol. 35, no. 4, pp. 512-526, April 2000.

[10] H. Nathanson, W. E. Newell, R. A. Wickstrom, and J. R. Davis, Jr., "The resonant gate transistor," *IEEE Trans. Electron Devices*, vol. ED-14, No. 3, pp. 117-133, March 1967.

[11] R. J. Matthys, *Crystal Oscillator Circuits*. New York: Wiley, 1983.

[12] D. B. Leeson, "A simple model of feedback oscillator noise spectrum," *Proc. IEEE*, vol. 54, pp. 329-330, Feb. 1966.

[13] A. H. Nayfeh and D. T. Mook, *Nonlinear Oscillations*. New York: Wiley, 1979.

[14] K. Wang, A.-C. Wong, and C. T.-C. Nguyen, "VHF free-free beam high-Q micromechanical resonators," *IEEE/ASME J. Microelectromech. Syst.*,vol. 9, no. 3, pp. 347-360, Sept. 2000.

[15] C. T.-C. Nguyen, "Micromechanical Signal Processors," Ph.D. Dissertation, Dept. of EECS, University of California at Berkeley, Dec. 1994.